J. Fluid Mech. (1985), *vol.* 158, *pp.* 177–197
Printed in Great Britain

The dynamics of waves at the interface between a viscoelastic coating and a fluid flow

By J. H. DUNCAN†, A. M. WAXMAN‡ AND M. P. TULIN§
Tracor Hydronautics, Inc., Pindell School Road, Laurel, Maryland 20747

(Received 23 July 1984 and in revised form 30 January 1985)

The dynamics of two-dimensional uniform wavetrains on the interface between a viscoelastic compliant coating and a boundary-layer flow are explored theoretically. The coating is treated as a single-layer isotropic Voigt material of finite thickness that is bonded to a rigid half-space. The flow is modelled first by potential theory and then modified to incorporate pressure phase shifts and magnitudes found in boundary-layer flow over wavy walls. The consideration of viscoelastic effects has led to an important dimensionless damping parameter $\gamma_t = C_t \tau_t / d$ (where τ_t is the strain relaxation time, C_t is the elastic shear-wave speed and d is the layer depth) that seems to have been overlooked by experimentalists. The flow and the damping are found to have dramatic effects on wave propagation. Using flow pressure and material-damping parameters typical of experiments, the results show that both upstream- and downstream-propagating waves exist at low flow speeds. At higher flow speeds, shorter waves can no longer propagate upstream. At still higher velocities, two instabilities, 'static divergence' and 'flutter', are found. Static divergence occurs for flow speeds above $2.86C_t$ and consists of slow waves moving with speeds of about $0.02C_t$. These results compare fairly well with published experimental data. Static divergence is found to be a damping instability for these coating systems. When the flow speed is increased further, the flutter instability appears consisting of waves with phase speeds about equal to C_t.

1. Introduction

The desire to reduce skin friction, flow noise and panel flutter has motivated a number of studies of the behaviour of waves at the interface between viscoelastic structures and boundary-layer flows. Most studies (see e.g. Bushell, Hefner & Ash 1977; Chyu & Au-Yang 1973; Dugundji, Dowell & Perkin 1963; Gislason 1971; Miles 1956) have involved experiments and theory for waves on relatively simple structures, such as membranes, free plates, and plates supported by springs and dampers. The experiments have shown the existence of instabilities at sufficiently high flow speeds, and these instabilities are predicted fairly well by the theories. A series of theoretical papers by Benjamin (1960, 1963, 1964) and Landahl (1962) examined the effects of compliant boundaries on the stability of laminar flow. These papers presented a general theory of the instabilities in fluid–elastic systems. Three classes of waves were

† Present address: Flow Research Company, 1320 Fenwick Lane, Silver Spring, Maryland 20910.
‡ Present address: Computer Vision Laboratory, Center for Automation Research, University of Maryland, College Park, Maryland 20742.
§ Present address: Department of Mechanical and Environmental Engineering, University of California at Santa Barbara, California 93106.

found, each supporting a different instability mechanism: class A (damping instabilities), class B (phase-lag instabilities), and class C (Kelvin–Helmholtz or flutter instabilities). The theory was then applied to flow over a coating-like structure consisting of a modified membrane model.

More recently, Hansen & Hunston (1974, 1983), Hansen *et al.* (1979) and Gad-el-Hak, Blackwelder & Riley (1984) have performed experiments to examine instabilities in systems of flow over thin layers of viscoelastic materials that are bonded to a rigid plate. The material used for the coatings was a plastisol gel. For turbulent flows, the experiments showed that at a sufficiently high flow speed (3 or more times the shear-wave speed of the solid, C_t), slowly moving unstable waves appeared on the coating surface. These waves, which are called static divergence waves (presumably in analogy to the static Kelvin–Helmholtz instability found in potential flow over panels of finite length – Dowell 1975), move with speeds of only a few percent of the shear-wave speed and have wavelengths of the order of the coating thickness. In the case of laminar flow over the coating, Hansen & Hunston (1983) found a similar instability, but with an onset flow speed of about $4.5C_t$, while Gad-el-Hak *et al.* (1984) were unable to find the instability at any flow speed.

In this paper a simple theory is presented to model the experiments on flow over viscoelastic coatings. Specifically, we calculate the dispersion relations for waves on homogeneous isotropic coatings consisting of Voigt materials that are attached to a rigid half-space on one side and bounded by a turbulent or laminar flow on the other. The flow and the coating are inviscidly coupled by the interfacial pressure and the normal velocity. A simple flow model is employed consisting of potential theory that is modified to incorporate pressure phase shifts and magnitudes found in turbulent or laminar flow over wavy walls. The dispersion curves resulting from this linear analysis are used to explore the physics of waves in the flow–coating system. It is realized that this simple model cannot describe the effects of the wall on waves that would exist in a boundary layer over a rigid surface. In the case of a simple wall model and a laminar flow Landahl & Kaplan (1965) have performed extensive numerical calculations of this type. However, our main goal is to elucidate the dynamics of the instabilities found in the published experimental studies under both laminar and turbulent flows, and, as the results will show, the present theory is adequate for this purpose. The dispersion curves can also be used to explore the generation of stable waves in the coating surface by turbulent pressure fluctuations, a subject that is at the heart of attempts to reduce turbulent skin friction with a compliant surface.

The paper is divided into three sections. In §2 a derivation of the dispersion relation is presented. The numerical results showing the dispersion curves as a function of flow speed and material properties are given and discussed in §3. Included are comparisons with the available experimental data. The concluding remarks are found in §4.

2. Theoretical analysis

In this section we derive dispersion relations for surface waves on a layer of homogeneous, isotropic Voigt material of uniform thickness d and infinite horizontal extent. On its lower boundary, the layer is attached to a rigid half-space. On its upper surface it is bounded by flowing water (see figure 1). At the interface between the fluid and the coating we consider a wave of the form

$$\eta = a\,\mathrm{e}^{\mathrm{i}k(x-ct)}, \tag{1}$$

where a is the amplitude, k is the wavenumber (2π divided by the wavelength λ) and c ($= c_r + \mathrm{i}c_i$) is the complex wave speed. The propagation speed of the wave is

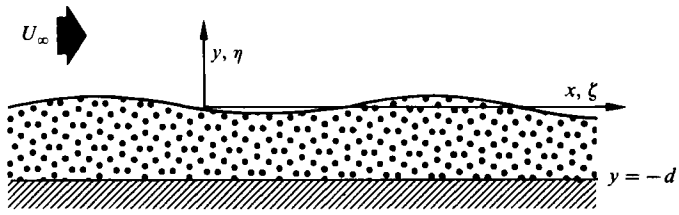

FIGURE 1. Layer schematic.

given by c_r and the wave growth rate by kc_i ($c_i > 0$ indicates a growing wave). The differential equation of motion governing small displacements in a Voigt material is (see Fung 1965)

$$\frac{\partial^2 \boldsymbol{\zeta}}{\partial t^2} = C_T^2 \nabla^2 \boldsymbol{\zeta} + (C_L^2 - C_T^2) \nabla(\nabla \cdot \boldsymbol{\zeta}), \tag{2}$$

where $\boldsymbol{\zeta} = \zeta \boldsymbol{i} + \eta \boldsymbol{j}$ is the displacement vector and ζ and η are the horizontal and vertical components (see figure 1). C_T and C_L are the complex shear and longitudinal wave speeds of the solid. Considering small displacements proportional to $e^{ik(x-ct)}$, we have

$$\left.\begin{aligned} C_T^2 &= C_t^2(1 - ikdC\gamma_t), \\ C_L^2 &= C_\ell^2\left(1 - ikdC\frac{C_t}{C_\ell}\gamma_\ell\right), \end{aligned}\right\} \tag{3}$$

where $C = c/C_t$, C_t and C_ℓ are the shear- and longitudinal-wave speeds in an ideal elastic solid, and γ_t and γ_ℓ are introduced as dimensionless damping ratios, defined by

$$\gamma_t = \frac{\tau_t C_t}{d}, \quad \gamma_\ell = \frac{\tau_\ell C_\ell}{d}. \tag{4}$$

The relaxation times τ_t and τ_ℓ indicate the dissipative properties of the material. For incompressible materials the damping properties are sometimes reported in terms of the loss tangent, $\tan\delta = \tau_t \omega_r$, where $\omega_r = c_r k$.

There are four boundary conditions for the present problem:

$$2\rho C_T^2 \frac{\partial \eta}{\partial y} + \rho(C_L^2 - 2C_T^2)\left(\frac{\partial \zeta}{\partial x} + \frac{\partial \eta}{\partial y}\right) = -P_f \quad (y = 0), \tag{5}$$

$$\rho C_T^2 \left(\frac{\partial \zeta}{\partial y} + \frac{\partial \eta}{\partial x}\right) = 0 \quad (y = 0), \tag{6}$$

$$\zeta = 0 \quad (y = -d), \tag{7}$$

$$\eta = 0 \quad (y = -d), \tag{8}$$

where ρ is the density of the coating and P_f is the surface pressure. Equations (5) and (6) are the linearized continuity-of-force conditions at the upper boundary. The calculations of Benjamin (1959) show that the variations in pressure over the wave profile far outweigh the variations in shear stress. Also, the flow pressure is much greater than the normal viscous stress. Thus in the present model we match the flow pressure and the vertical stress component in the coating, while the shear stress at the interface is taken to be zero. Conditions (7) and (8) state that there is no horizontal or vertical displacement at the lower boundary $y = -d$.

The solution of these equations is accomplished by breaking the displacement field

ζ into two parts: one with zero curl, ζ_ℓ, and one with zero divergence, ζ_t (see Fung 1965, p. 184). Thus we have

$$\left.\begin{aligned}\zeta = \zeta_\ell + \zeta_t &= \frac{\partial\phi}{\partial x} + \frac{\partial\psi}{\partial y},\\ \eta = \eta_\ell + \eta_t &= \frac{\partial\phi}{\partial y} - \frac{\partial\psi}{\partial x},\end{aligned}\right\} \tag{9}$$

where ϕ and ψ are scalar functions of time and position. When these definitions are substituted into (2) and the curl and divergence of the equation are taken separately, we obtain

$$\nabla^2\left(\nabla^2\phi - \frac{1}{C_L^2}\frac{\partial^2\phi}{\partial t^2}\right) = \nabla^2\overline{\Phi} = 0 \tag{10}$$

from the divergence, and

$$\nabla^2\left(\nabla^2\psi - \frac{1}{C_T^2}\frac{\partial^2\psi}{\partial t^2}\right) = \nabla^2\overline{\Psi} = 0 \tag{11}$$

from the curl. Note that the equations have been divided by C_L^2 and C_T^2. At complex frequencies where $C_T = 0$ or $C_L = 0$ this introduces artificial poles into the implicit function defining the dispersion relation. Care is taken to avoid these poles in the final results.

The solutions to (10) and (11) are greatly simplified if $\overline{\Phi}$ and $\overline{\Psi}$ can be taken equal to zero. In the Appendix we show that this is the case for $c \neq 0$. For the purely static case, $c = 0$, it is demonstrated that both $\overline{\Phi}$ and $\overline{\Psi}$ are nonzero. However, the criterion that follows for these static solutions is equivalent to that obtained with $\overline{\Phi} = \overline{\Psi} = 0$ in the limit $c = 0$. Thus, without loss of generality, we propose to derive the dispersion relation with $\overline{\Phi} = \overline{\Psi} = 0$. We look for solutions of the form

$$\left.\begin{aligned}\phi &= \hat{\phi}(y)\,e^{ik(x-ct)},\\ \psi &= \hat{\psi}(y)\,e^{ik(x-ct)},\end{aligned}\right\} \tag{12}$$

and, after substituting these into (10) and (11), we have

$$\left.\begin{aligned}\frac{d^2\hat{\phi}}{dy^2} - k^2\left(1 - \frac{c^2}{C_L^2}\right)\hat{\phi} &= 0,\\ \frac{d^2\hat{\psi}}{dy^2} - k^2\left(1 - \frac{c^2}{C_T^2}\right)\hat{\psi} &= 0.\end{aligned}\right\} \tag{13}$$

The solutions of these ordinary differential equations are

$$\hat{\phi} = A_1\frac{\sinh\alpha ky}{k\alpha} + B_1\cosh\alpha ky, \tag{14}$$

$$\hat{\psi} = A_2\frac{\sinh\beta ky}{\beta k} + B_2\cosh\beta ky, \tag{15}$$

where

$$\alpha^2 = 1 - \frac{c^2}{C_L^2}, \tag{16}$$

$$\beta^2 = 1 - \frac{c^2}{C_T^2}. \tag{17}$$

These solutions are to be substituted into the boundary conditions (5)–(8). Before doing this, let us first determine a form for the surface pressure P_f. For potential flow

of speed U_∞ and density ρ_f over a boundary of the form of (1), the pressure can be shown to be

$$P_{\text{pot}} = -\rho_f ak(U_\infty - c)^2 \, e^{ik(x-ct)}. \tag{18}$$

We model the actual mean-pressure distribution in the turbulent or laminar boundary-layer flow by modifying the above potential-flow pressure equation to allow for a reduced magnitude and phase change. This is a reasonable technique in view of the experimental data of Kendall (1970) and the theoretical work of Benjamin (1959) and Balasubramanian & Orszag (1983). Thus we have

$$P_f = -K_p \rho_f ak(U_\infty - c)^2 \, e^{i[\theta_p + k(x-ct)]}. \tag{19}$$

For a given boundary layer the constants K_p and θ_p are functions of wavenumber and phase speed. In the present work values are taken from the experimental data of Kendall (1970) for turbulent flows and from Balasubramanian & Orszag (1983) for laminar flows. We believe that this relatively simple modelling of the fluid forces on the coating includes the essential physics for the phenomenon considered here. Note, however, that this model would not be able to predict the effect of the coating on instabilities in a boundary-layer flow, such as Tollmien–Schlichting waves.

After substituting (9), (12), (14) and (15) into the boundary conditions, we have four homogeneous algebraic equations for the unknowns A_1, B_1, A_2 and B_2. The dispersion relation for surface waves in the solid/fluid system results from setting the determinant of the coefficients equal to zero:

$$\begin{aligned}\frac{\rho_f}{\rho} K_p \left(\frac{U_\infty}{C_t} - \frac{c}{C_t}\right)^2 e^{i\theta_p} (\beta^2 - 1) \left(\frac{1}{\beta} \cosh \alpha kd \sinh \beta kd - \alpha \cosh \beta kd \sinh \alpha kd\right) \\ - 4 \frac{C_T^2}{C_t^2} (1 + \beta^2) + \frac{C_T^2}{C_t^2} (1 + \beta^2)^2 \left(\cosh \alpha kd \cosh \beta kd - \frac{1}{\alpha\beta} \sinh \alpha kd \sinh \beta kd\right) \\ + 4 \frac{C_T^2}{C_t^2} (\cosh \alpha kd \cosh \beta kd - \alpha\beta \sinh \alpha kd \sinh \beta kd) = 0. \end{aligned} \tag{20}$$

This dispersion relation is a complicated implicit function that is analytic in the complex phase speed c, except at the singularities introduced by dividing the equations of motion by C_L^2 and C_T^2 (see comment after (10) and (11)). The numerical results presented in §3 were obtained using a contour-integration method to find the complex zeros of the dispersion function. This method is based on the work of Delves & Lyness (1967).

3. Results and discussion

It is convenient to present the results in several parts. First, in §3.1, the physics of the interfacial waves are discussed in terms of the wave classes identified by Benjamin (1963) and Landahl (1962). Then, in §3.2, dispersion curves for a potential flow over a purely elastic incompressible coating are presented, and regions of the curves that belong to the three separate wave classes are identified. The effect of material damping and pressure distributions that simulate boundary-layer flows are presented in §3.3. Finally, in §3.4, the results of the model are compared with existing experimental data. In all cases the coating materials have been taken as nearly incompressible, $C_\ell/C_t = 70$ and $\gamma_\ell = 0$.

3.1. *Wave classes*

Before discussing the numerical results, it will be useful to briefly review the findings of Benjamin (1960, 1963, 1964) and Landahl (1962). Their work emphasized the

stability of laminar flow over membranes, but their general concepts are applicable to the present case as well. The authors found three separate classes of waves (designed A, B and C) in the fluid/coating system. Classes A and B are neutrally stable in an ideal system (with no damping and no pressure phase lags), while class C, flutter, is unstable. Each class can be identified by the sign of the 'activation energy' ΔE defined by Benjamin (1963) as the change in kinetic and potential energy of the coating plus the change in energy of the flow due to the work done on the coating by conservative forces only. In the present case we have

$$\Delta E = \frac{1}{\lambda}\int_x^{x+\lambda}\int_{-d}^{\zeta|_{y=0}} (\mathrm{SE}+\mathrm{KE})\,\mathrm{d}y\,\mathrm{d}x + \frac{1}{\lambda}\int_x^{x+\lambda} W_{\mathrm{cons}}\,\mathrm{d}x, \tag{21}$$

where KE and SE, the kinetic and elastic-strain energy of the coating respectively, are defined as

$$\mathrm{SE} = \frac{\rho}{2}\left\{C_l^2\left[\left(\frac{\partial\xi}{\partial x}\right)^2+\left(\frac{\partial\eta}{\partial y}\right)^2\right]+2\,(C_l^2-2C_t^2)\frac{\partial\xi}{\partial x}\frac{\partial\eta}{\partial y}+C_t^2\left(\frac{\partial\xi}{\partial y}+\frac{\partial\eta}{\partial x}\right)^2\right\}, \tag{22}$$

$$\mathrm{KE} = \frac{\rho}{2}\left[\left(\frac{\partial\xi}{\partial t}\right)^2+\left(\frac{\partial\eta}{\partial t}\right)^2\right] \tag{23}$$

(note that the use of the lower-case subscripts in (22) is intentional, see (3)). To derive the conservative work term we follow Benjamin's (1963) derivation of the work done by a potential flow, substituting the conservative part of our pressure term

$$P_{\mathrm{cons}} = -K_p\rho_f ak(U_\infty - c)^2\cos\theta_p\,\mathrm{e}^{\mathrm{i}k(x-ct)} \tag{24}$$

for the potential-flow pressure in his calculation. Thus we find

$$\frac{1}{\lambda}\int_x^{x+\lambda} W_{\mathrm{cons}}\,\mathrm{d}x = \tfrac{1}{4}K_p\rho_f k\cos\theta_p(cc^* - U_\infty^2)\,\tilde{\eta}^2, \tag{25}$$

where $\tilde{\eta} = a\,\mathrm{e}^{kc_i t}$. Note that when $K_p = 1$ and $\theta_p = 0$ (a potential flow) this reduces to minus Benjamin's expression for the energy loss of the flow (his expression (A 6)) with his wave amplitude $f(t)$ taken as $ae^{kc_i t}$ and without the restriction that $\dot{f} = 0$ at time t. This generalization to growing waves is necessary in the calculation of ΔE for unstable waves and, as will be seen in §3.2, gives the correct result for class C waves, i.e. $\Delta E = 0$. The sign of ΔE is used to define the three wave classes. It is negative for class A waves, positive for class B waves, and zero for class C waves. For classes A and B the magnitude of ΔE is proportional to a^2. In each wave class the irreversible energy-transfer processes (damping and pressure phase shifts) affect the stability of the fluid–coating system differently.

Let us consider the effect of damping on the three classes of waves. For this discussion the pressure phase lag (from the potential-flow case) is assumed to be zero. In all wave classes damping removes mechanical energy from the solid. Thus, as any of these waves propagate, damping tends to decrease ΔE. In each class the wave amplitude behaves differently to accommodate this decrease. The most familiar case is class B, where the wave amplitude decreases with decreasing system energy. Here damping tends to make the wave decay. For class A waves, where the wave amplitude grows as ΔE becomes more negative, the effect of damping is reversed: as the wave propagates, its amplitude tends to grow to accommodate the energy decrease. In class C waves, the primary causes of wave growth and decay are reversible processes. However, in this region damping does have a small effect similar to that found in class B waves.

Pressure phase lags lead to irreversible energy transfer between the interfacial-wave system and the uniform flow at infinity. In the case of downstream-running waves moving slower than the flow, the transfer of energy is from the flow to the wave system. Thus, as the wave propagates, its energy ΔE must increase. This implies decay for class A waves and growth for class B waves. Again, in class C, the main effects are the reversible processes, but pressure effects have the same tendency as in class B. In the case of upstream-running waves the energy transfer is from the wave system to the flow. This energy drain affects the three wave classes in the same direction as material damping.

The dispersion curves presented in §3.2 can be divided into portions that belong to the three wave classes identified above. The location and existence of portions corresponding to each class will depend on the flow speed, pressure factors and damping parameters. Thus, for instance, strong damping not only destabilizes class A waves but can also affect the existence of a class A portion of the dispersion curve. This rather complicated situation will be clearly demonstrated by the results presented below.

3.2. *Dispersion curves – potential flow over a purely elastic coating*

Figures 2–5 show the dispersion curves for a potential flow ($K_p = 1$, $\theta_p = 0$) over a purely elastic coating ($\gamma_t = 0$). Each figure contains a plot of wave phase speed $C = c/C_t$ versus wavenumber kd for a single flow speed U_∞/C_t. Figures 3–5 also contain plots of ΔE. Let us first examine the zero-flow-speed results shown in figure 2. Note that the values of C are purely real, as one would expect. These dispersion curves consist entirely of class B waves, since the energy of the disturbed system is greater than that of the undisturbed system ($\Delta E > 0$). The curves are symmetric about the line $C = 0$ and show a modal behaviour. Thus, for any wavenumber, there are an infinite number of discrete positive–negative pairs of wave speeds that satisfy the dispersion relation. The higher the wave speed for a given kd (defined as higher mode), the more complex the vertical distribution of displacement in the coating. Note that the mode 1 curves (lowest $|C|$) are asymptotic to $C = 0.837$ as $kd \to \infty$, i.e. infinite depth. This limit should be compared with the results of Rayleigh (1885), who calculated the speed of surface waves on a semi-infinite solid bounded by a vacuum. Both results are dispersionless (C is a constant), but in the Rayleigh-wave case the speed is 0.955. The lower wave speed in the present case is a result of the added mass of the bounding fluid. Note that in figure 2 there are no waves with $|C| < 0.837$.

The dispersion curves for a flow speed of C_t are shown in figure 3. Again, the values of C are real. Note that the downstream-running (positive-C) waves exhibit only minor changes from the no-flow case. On the other hand, the upstream-running (negative-C) mode 1 curve shows a large increase in speed (toward zero). Note that the curves for ΔE are positive everywhere, and thus are of class B. When the flow speed is increased to $1.6C_t$ (figure 4) C is still real everywhere, but the mode 1 upstream-running curve corresponds to a downstream-running wave for $kd > 2.4$. An analysis for large kd has shown that the mode 1 upstream-running curve first crosses the $C = 0$ axis at $kd = \infty$ for $U_\infty/C_t = 1.41$. Note that the ΔE curves show that the downstream branch is a class B wave for all kd, as is the part of the upstream branch that is still running upstream. The portion of the upstream branch that is running downstream has become class A ($\Delta E < 0$).

The analysis for large kd also shows that the mode 1 upstream curve meets the downstream curve at $kd = \infty$ for a flow speed of $1.79C_t$. When the curves meet, the two values of C becomes a complex-conjugate pair ($C = C_r \pm iC_i$) corresponding to

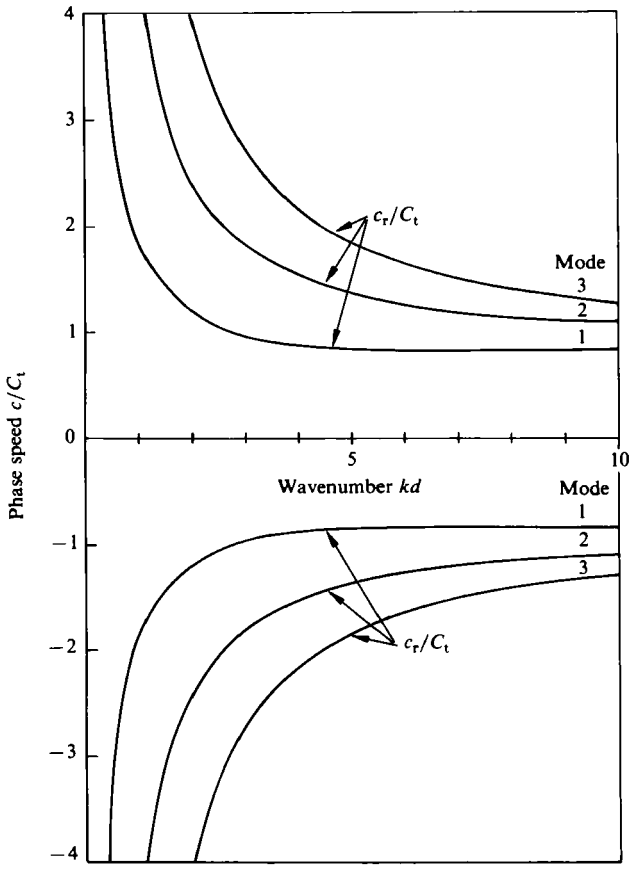

FIGURE 2. Wave speed versus wavenumber for a potential flow over an elastic coating; $U_\infty/C_t = 0$, $K_p = 1$, $\theta_p = 0$, $\gamma_t = 0$, $\rho_t/\rho = 1$.

growing and decaying waves. The situation at a flow speed of 1.85 is shown in figure 5. Note that ΔE goes to zero where the real-phase-speed curves meet ($kd = 3.8$, $C = 0.7$), and remains so for the complex parts of the curves (class C). This is a rather strong instability with a growth rate kdC_i greater than 0.8. For higher flow speeds the waves become unstable at lower kd, and their growth rate increases. Note that at the flow speed $1.85C_t$ (figure 5) all three classes of waves are present. The stability of these three wave classes in the presence of damping and pressure phase lags will be examined in §3.3.

In experiments (see e.g. Hansen & Hunston 1974), the first instability seen with increasing flow speed is static divergence, which consists of waves with phase speeds of about $0.03C_t$. Note that, in the above results with no material damping or pressure phase lags, there is no indication of the observed unstable waves. This result should be contrasted with the instabilities in a system of potential flow over a flat plate of finite extent. In the latter case, under some conditions, a Kelvin–Helmholtz (class C) instability appears with zero phase speed (Dowell 1975). Presumably, the coating instability was termed static divergence because of its qualitative similarity to the static divergence of plates. In §3.4 we will see that it is actually a damping instability (class A).

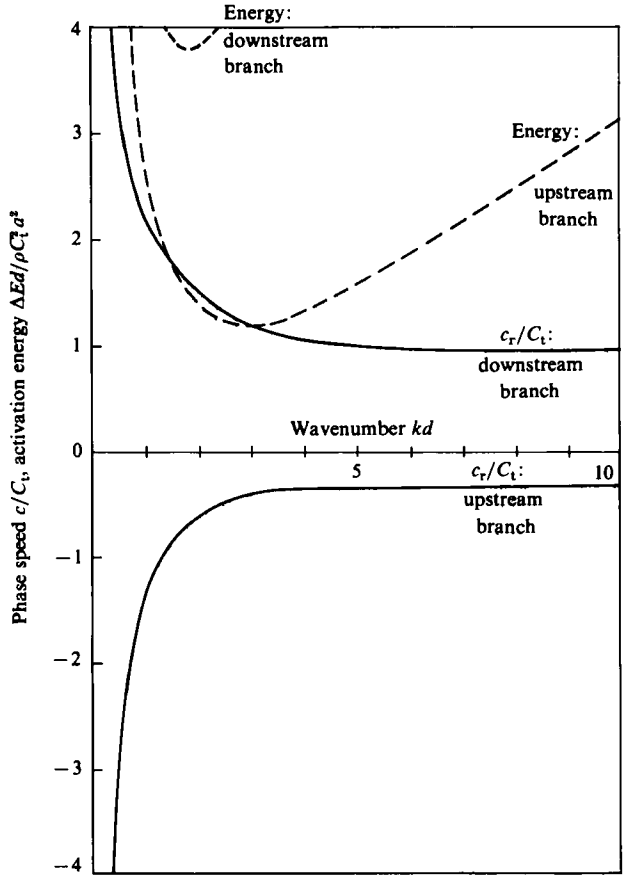

FIGURE 3. Mode 1 wave speed and activation energy versus wavenumber for a potential flow over an elastic coating; $U_\infty/C_t = 1$, $K_p = 1$, $\theta_p = 0$, $\gamma_t = 0$, $\rho_t/\rho = 1$.

When calculations are performed for a conservative pressure ($\theta_p = 0$) with reduced magnitude ($K_p < 1$) the wave classes remain qualitatively the same, but the flow speed at which the upstream dispersion curve crosses the zero axis (the onset of class A waves) and the flow speed at which the upstream and downstream branches meet (the onset of class C waves) are both increased. Since the upstream branch first crosses the zero axis at $kd = \infty$ a large-wavenumber analysis can be used to show that the flow speed for the onset of class A waves is

$$\left.\frac{U_\infty}{C_t}\right|_{\text{class A onset}} = \left(\frac{2}{K_p}\frac{\rho}{\rho_t}\right)^{\frac{1}{2}}. \tag{26}$$

Thus, for instance, with $K_p = 0.25$ we have $U_\infty/C_t|_{\text{class A onset}} = 2.83$. The onset of class C waves is correspondingly increased as K_p is reduced.

3.3. *Dispersion curves – the effects of material damping and pressure phase shifts*

In this subsection we discuss the modifications in the reversible results shown above when material damping and pressure phase shifts are present. This section will serve to verify the ΔE calculations and our understanding of the physics of the waves. The values of the damping and pressure coefficients used in this section were chosen for

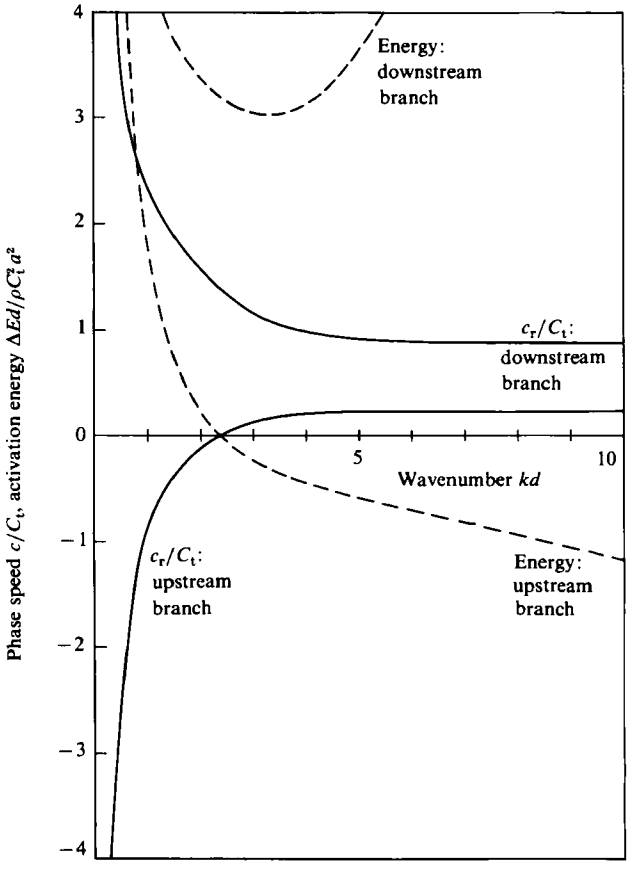

FIGURE 4. Mode 1 wave speed and activation energy versus wavenumber for a potential flow over an elastic coating; $U_\infty/C_t = 1.6$, $K_p = 1$, $\theta_p = 0$, $\gamma_t = 0$, $\rho_t/\rho = 1$.

illustrative purposes only. Let us first look at the effect of damping. Figure 6 contains the dispersion curves for a flow speed of $1.85C_t$ and a damping ratio of 0.01. The corresponding purely elastic case was discussed previously (see figure 5). At small wavenumbers the damping has caused the growth and decay of the neutrally stable class A and B waves of the purely elastic case. For the class B part of the downstream branch ($\Delta E > 0$, see figure 5) the damping has induced wave decay (negative C_i). For the upstream branch the portion that is class B also shows wave decay, while the class A portion ($\Delta E < 0$) shows wave growth. The class C portion of the curves in figure 6 also shows changes when damping is added. For the downstream branch, damping has increased the real part and decreased the already negative imaginary part. For the upstream branch, damping has decreased the real part of C and has had little effect on the imaginary part. These results are in agreement with the discussion given in §3.1. When the damping is increased to 0.05 (see figure 7), these effects remain similar, except for the class C portion of the upstream branch. The additional damping causes the growth rate to increase – the behaviour of a class A wave. Thus it can be seen that sufficient damping not only causes the effects described in §3.1 but can also change the class of some parts of the dispersion curves.

The effects of the pressure phase shift are shown in the dispersion curves of figure 8 ($U_\infty/c_t = 1.85$, $\gamma_t = 0$, $\theta_p = -5°$, $K_p = 1$). Here again, the irreversible process has

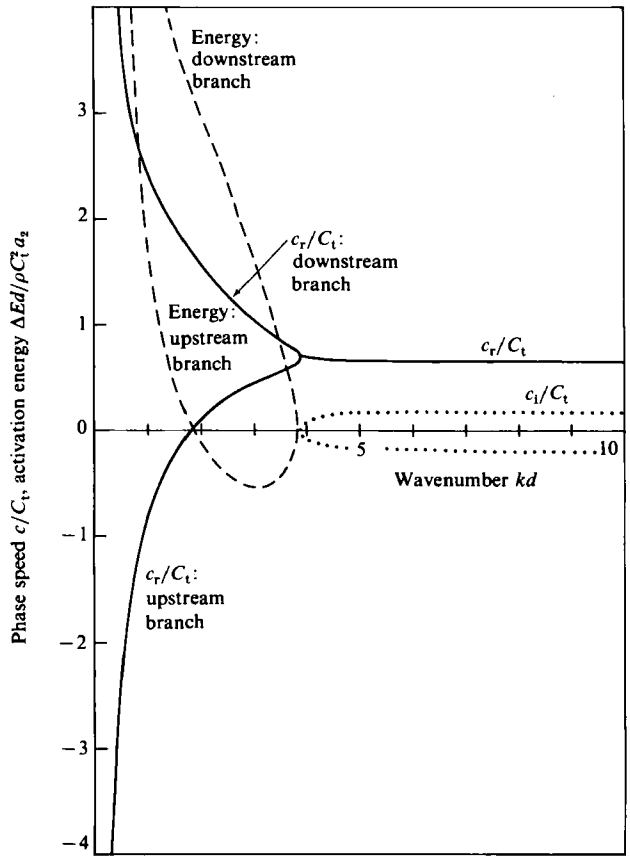

FIGURE 5. Mode 1 wave speed and activation energy versus wavenumber for a potential flow over an elastic coating $U_\infty/C_t = 1.85$, $K_p = 1$, $\theta_p = 0$, $\gamma_t = 0$, $\rho_t/\rho = 1$.

affected the stability of the otherwise neutral class A and B waves. The downstream-branch class B waves obtain a positive growth rate, the class A portion of the upstream branch (which is actually running downstream) is decaying, and the class B portion of the upstream branch is decaying also. In the class C portion of the curves in figure 8 the pressure phase shift has caused the downstream branch to increase its growth rate, as expected of a class C wave. However, the upstream branch decreases its growth rate, again showing the behaviour of a class A wave.

From the above discussion one can see that for the upstream-running waves of the upstream branch both damping and pressure phase shifts cause the waves to decay, while for all the downstream-running waves the two effects are in opposition regardless of wave class. Thus the stability of a given range of wavenumbers can only be determined for detailed conditions. Calculations for comparison with existing experimental data are presented in §3.4.

3.4. *Comparison with experimental results*

Hansen & Hunston (1974, 1983), Hansen *et al.* (1979) and Gad-el-Hak *et al.* (1984) have performed experiments with laminar and turbulent flows over coatings consisting of plastisol gels. These materials have extremely complex viscoelastic properties and are characterized by high damping (Hunston, Yu & Bullman 1984). The flows were

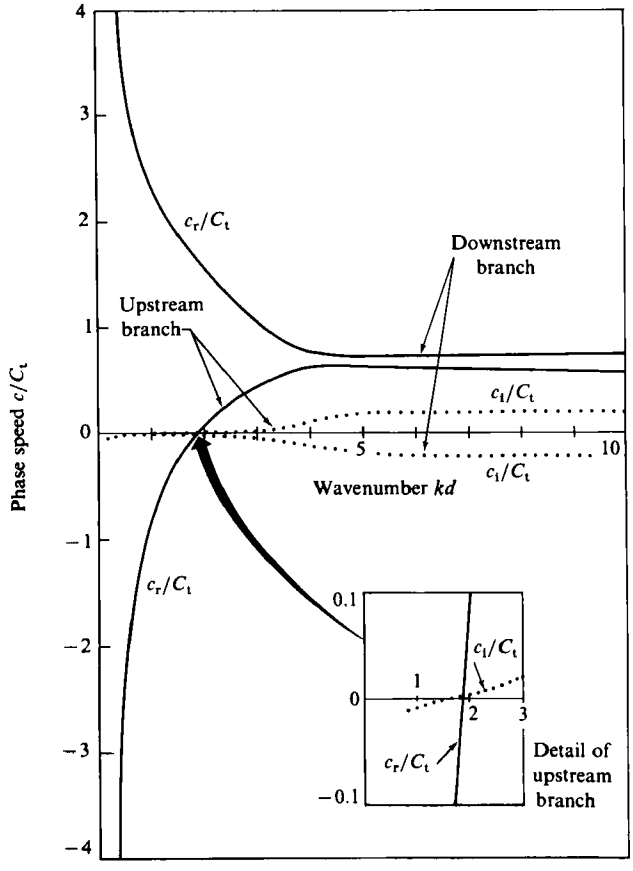

FIGURE 6. Mode 1 wave speed versus wavenumber for a potential flow over a viscoelastic coating; $U_\infty/C_t = 1.85$, $K_p = 1$, $\theta_p = 0$, $\gamma_t = 0.01$, $\rho_f/\rho = 1$.

produced in different ways: Hansen & Hunston used a rotating-disk apparatus, Hansen *et al.* used a flat plate in a recirculating water channel (and included some of the previous rotating-disk data) and Gad-el-Hak *et al.* used a flat plate in a towing tank. In all turbulent-flow cases, when the flow speed was increased beyond a critical value, slowly moving unstable waves appeared on the coating surface. Hansen & Hunston also found the instability under laminar flow conditions, while Gad-el-Hak *et al.* did not. This instability has been named static divergence. At still higher flow speeds in the experiments of Gad-el-Hak *et al.*, unstable waves with greater phase speeds appeared. Calculations for comparison with the experimental results of both the slow and fast waves are presented below.

In order to compare the calculations with the experiments, we must determine appropriate values for the damping ratio and the pressure coefficients. In our rather simple model, these coefficients are constants. In any boundary-layer flow the pressure coefficients K_p and θ_p are continuous functions of wave speed and wavenumber for a given boundary-layer velocity profile, while τ_t and C_t depend on frequency for the plastisol material used in the experiments.† Thus, to apply the

† The frequency dependence of C_t and τ_t indicates that the Voigt model does not give an accurate representation of the plastisol material. It is used here because we believe it contains the essential physics to model the overall phenomenon while maintaining mathematical simplicity.

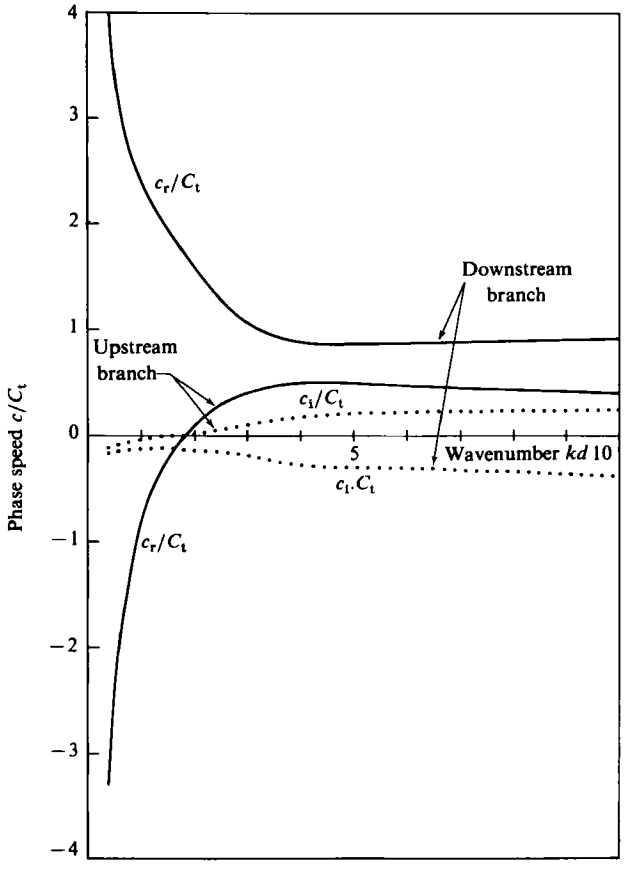

FIGURE 7. Mode 1 wave speed versus wavenumber for a potential flow over a viscoelastic coating, $U_\infty/C_t = 1.85$, $K_p = 1$, $\theta_p = 0$, $\gamma_t = 0.05$, $\rho_f/\rho = 1$.

model, we must choose the material and pressure coefficients to correspond to average values for the boundary layer, coating properties and wave characteristics found experimentally. For the pressure coefficients, we have chosen two sets of values to study static divergence under laminar and turbulent boundary layers. The corresponding experiments are characterized by slow wave speeds (at most a few percent of C_t or U_∞). For turbulent boundary layers in Gad-el-Hak *et al.* the wavelengths at onset ranged from 3.0 to 8.5 times the displacement thickness δ^*, while in Hansen *et al.* for the flat-plate data we estimate $\lambda/\delta^* = 20$–40. For comparison with these results, we have chosen $K_p = 0.25$ and $\theta_p = -10°$ from Kendall's (1970) experimental data on turbulent flow over wavy walls. These data, which are the most appropriate available, are for λ/δ^* in the range 14–20, midway between the experiments of Gad-el-Hak *et al.* and Hansen *et al.* (see table 1). For static divergence under laminar-flow conditions we have used the theoretical work of Balasubramanian & Orszag (1983) and chosen the values $K_p = 0.067$ and $\theta_p = -30.4°$ for $\lambda/\delta^* = 12$. These values correspond to the experiment of Gad-el-Hak *et al.* To study the stability of the faster-moving waves with phase speeds of about 0.3 times the flow speed, we have again used Kendall's data and chosen $K_p = 0.25$ and $\theta_p = -20°$.

As for the material properties, the experimental papers have scaled all results and experimental conditions with the layer depth and a shear-wave speed taken from a

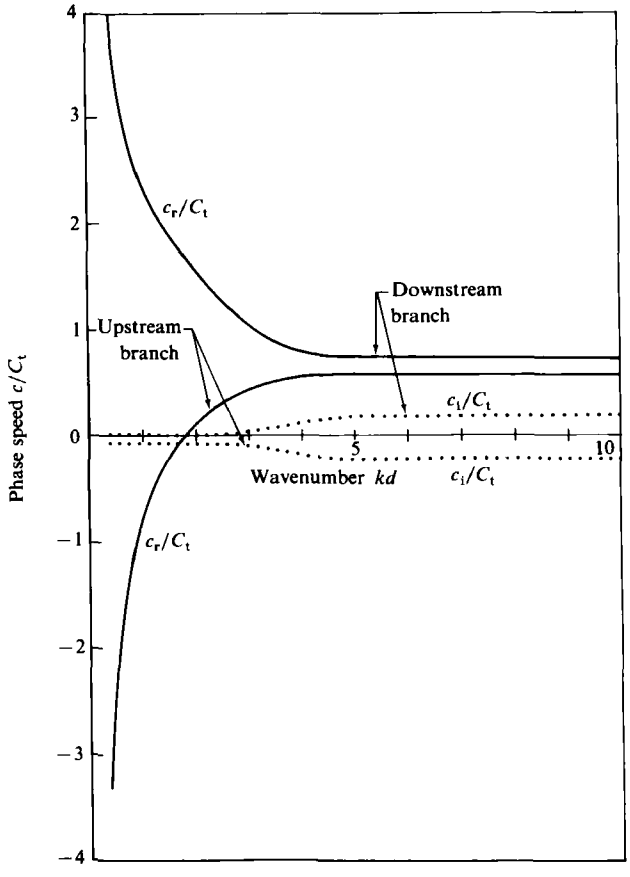

FIGURE 8. Mode 1 wave speed versus wavenumber for a flow with phase shift over an elastic coating; $U_\infty/C_t = 1.85$, $K_p = 1$, $\theta_p = -5°$, $\gamma_t = 0$, $\rho_f/\rho = 1$.

	λ/δ^*	$(U_\infty/C_t)_{onset}$	$(c_r/U_\infty)_{onset}$
Theory	14–20†	2.86	0.007 at $\gamma_t = 3$
Hansen *et al.* (1979)	20–40	3‡	0.008–0.012
Gad-el-Hak *et al.* (1984)	3–8.5	4.5–8.0	0.004–0.008

† In the theory K_p and θ_p are obtained from Kendall's (1970) data, which are for the quoted range of λ/δ^*.

‡ The rotating-disk data give $(U_\infty/C_t)_{onset} = 3.3$.

TABLE 1. Experimental and theoretical values for static divergence – turbulent flow over a flat plate

static measurement of the shear modulus for each coating. In an attempt to compare our results with the experiments, we have obtained approximate values of γ_t from the material properties given by Hunston *et al.* (1984). These measurements include the shear-wave speed and loss tangent as a function of frequency. Accordingly, two values of the damping parameter have been chosen as typical of the experiments:

3 for the static divergence comparison (low frequency) and 0.3 for the faster-moving waves (high frequency). For the static divergence results, we have also varied the damping ratio from 1 to 100 to cover all possible experimental conditions.

Slow-wave results

Let us first examine the slow-wave results and then look at the higher-speed case. Calculations for the turbulent-boundary-layer conditions are given in figure 9. The figure contains curves of wave phase speed $c_r/C_t = C_r$ growth rate $c_i\, kd/C_t = \omega_i$ and activation energy $\Delta E\, d/\rho C_t^2 a^2$ versus wavenumber for two flow speeds $U_\infty/C_t = 2.5$ and 3.5. Only the portion of the dispersion curves around $C = 0$ are plotted. Note that C_r has been multiplied by 100 for plotting purposes. These dispersion curves correspond to the upstream-running branches of the reversible results in figures 2–5. For the lower flow speed the C_r curve crosses the zero axis at a wavenumber of about 1.2; and, for wavenumbers greater than 1.2, C_r is positive. Since the corresponding ω_i values are negative and the ΔE values are positive for all kd, it appears that these are stable class B waves. At the higher flow speed the growth rate and phase speeds are above their low-flow-speed counterparts. As the wavenumber increases, the ΔE curve changes sign from positive to negative at the wavenumber where the growth rate changes from negative to positive, thus indicating a class A instability. The growth rate of this instability ($\omega_i = 0.2$) is rather high considering its low phase speed ($C_r = 0.02$ at $kd = 4$). Thus we find that the ratio of the wave period to the growth timescale ω_i/kdC_r is equal to 2.5. The onset flow velocity for this instability is $U_\infty/C = 2.86$, and it occurs for high wavenumbers first.

Table 1 contains the onset flow velocities and wave speeds for the theory and the existing flat-plate experimental data. The theoretical onset flow velocity corresponds well to the experimentally determined values for static divergence found by Hansen *et al.* (1979): $U_\infty/C_t = 3$ for the flat-plate experiments. The paper by Gad-el-Hak *et al.* (1984) shows the onset velocity to vary with coating thickness. Their values range from $U_\infty/C_t = 4.5$ at a thickness of 0.71 cm to about 8 at 0.15 cm. Noting that the damping ratio varies as $1/d$, we have examined the dispersion curves to find the onset velocity of static divergence for the range $1 < \gamma_t < 100$. The results show the onset velocity to be a constant for the entire range of γ_t. We suspect that the model's poor performance in predicting the magnitude and trend of the data of Gad-el-Hak *et al.* is the result of using a single set of values for the pressure coefficients. The range of λ/δ^* for these experiments is considerably lower than the values in Kendall's experiments, from which we have obtained our coefficients. Thus a lower value of K_p would be more appropriate to the results of Gad-el-Hak *et al.*, and this value should be decreased with coating thickness, i.e. wavelength. We compute that $K_p = 0.1$ would result in an onset velocity of $4.5C_t$, the value obtained experimentally at the largest coating thickness. The onset velocities of Hansen *et al.*, which are for λ/δ^* higher than Kendall's data, indicate that the pressure parameters are accurate.

The calculated speed of the unstable waves compares well with the experimental values (see table 1). At onset we find $c_r/C_t = 0.02$ or $c_r/U_\infty = 0.007$. The experiments of Hansen *et al.* find $c_t/U_\infty = 0.008$–0.012. The values found by Gad-el-Hak *et al.* are quite similar ($c_r/U_\infty = 0.004$ for the 0.24 cm coating to $c_r/U_\infty = 0.008$ for the thickest coating).

The comparison between the predicted wavelength of static divergence and the experimentally obtained values is not as satisfying. The present model predicts that as the flow speed is increased the growth rate first becomes positive at $kd = \infty$. At higher flow speeds the growth rate is rather flat, with $kd\omega_i$ attaining its maximum

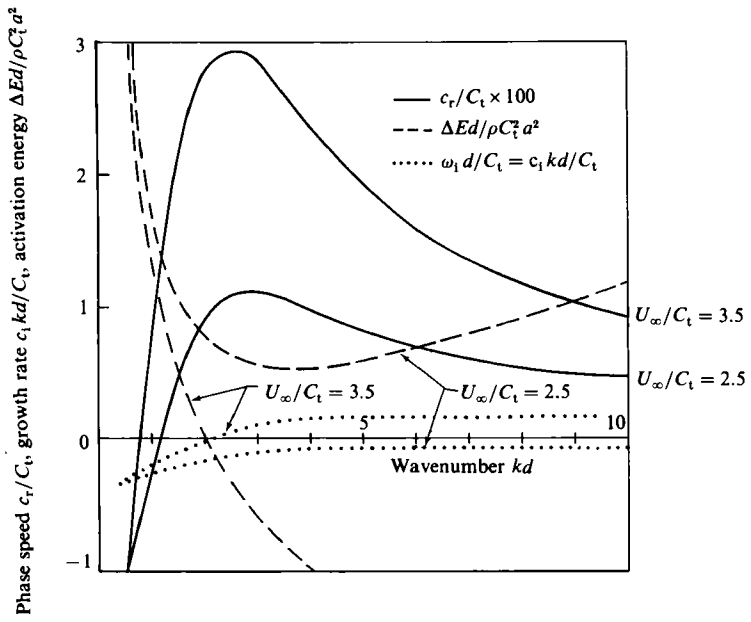

FIGURE 9. Wave speed, growth rate and activation energy versus wavenumber for comparison with slow-wave experimental measurements – turbulent boundary layer; $K_p = 0.25$, $\theta_p = -10°$, $\gamma_t = 3$, $\rho_t/\rho = 1$.

value at $kd = \infty$. It is believed that the use of a more accurate pressure model would produce a maximum growth rate at a finite wavenumber. As was explained above, in the present model, the same coefficient is applied to all waves regardless of their length compared with the boundary-layer thickness. In reality, waves of shorter length (larger k) have smaller K_p. Gad-el-Hak *et al.* have measured the wavelength of the static divergence waves. They found that the wavelength increased with d. For a general comparison, we have used the wavelength of the zero-crossing of the C_r curve (see (A 7) in the Appendix) to compare with the experimental data. If the observed waves are indeed the result of the class A instability, then they should have kd-values that are higher (or λ/d-values that are lower) than the theory. The data of Gad-et-Hak *et al.* are plotted in figure 10 along with the zero-crossing results showing the validity of the model.

A plot similar to that in figure 9 is given in figure 11, but this time for a laminar boundary layer. The behaviour in figure 11 is qualitatively similar to that in figure 9, but the onset velocity for static divergence is much higher in the laminar-flow case. The ΔE curves, which have been omitted to avoid clutter, again verify that the instability is class A. The calculations predict an onset flow velocity of $5.92C_t$ or 2.1 times the value in the turbulent case. Note also that at about $0.6C_t$ above the onset flow speed the phase speed of the laminar case is as much as 2.5 times larger than in the turbulent case, while the growth rate is 2.5 times smaller. The increase in onset speed for the laminar case is primarily the result of the smaller pressure coefficient; a higher flow speed is needed to pull the upstream branch of the dispersion curve up so that the high-kd part becomes a downstream, unstable class A wave.

In the rotating-disk experiments of Hansen & Hunston (1983) it was found that the onset flow velocity in the laminar-flow case increased to 1.5 times the turbulent value. (The change from turbulent to laminar conditions was brought about by

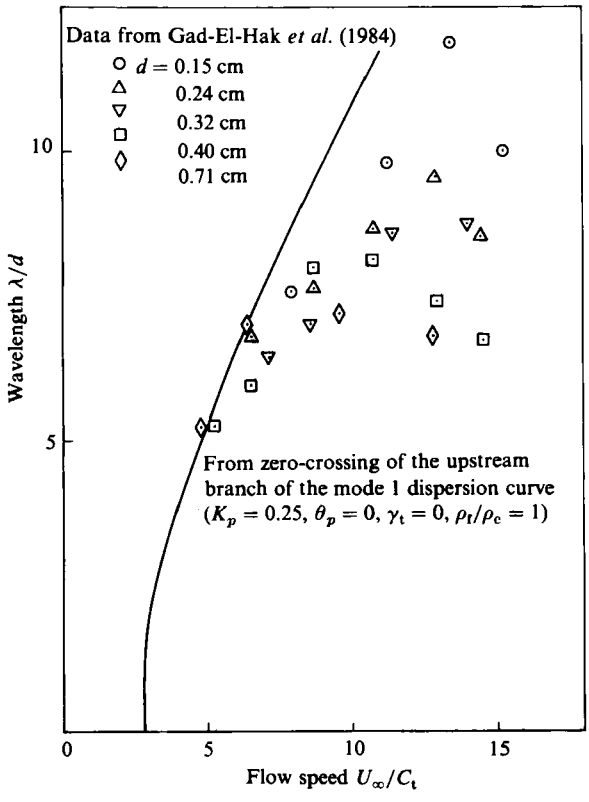

FIGURE 10. Comparison of measured wavelength of static divergence from Gad-el-Hak *et al.* (1984) with wavelength at zero-crossing of upstream dispersion curve.

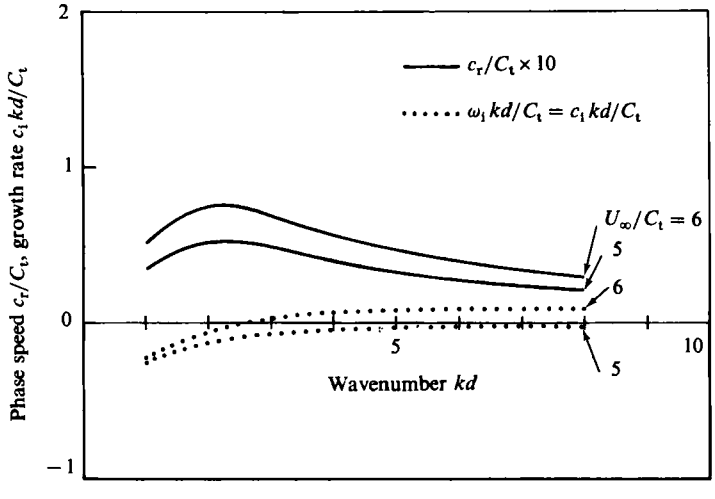

FIGURE 11. Wave speed and growth rate versus wavenumber for comparison with slow-wave experimental measurements – laminar boundary layer; $K_p = 0.067, \theta_p = -30.4°, \gamma_t = 3, \rho_f/\rho_c = 1$. (Note the difference in scale factor for c_r/C_t from figure 9.)

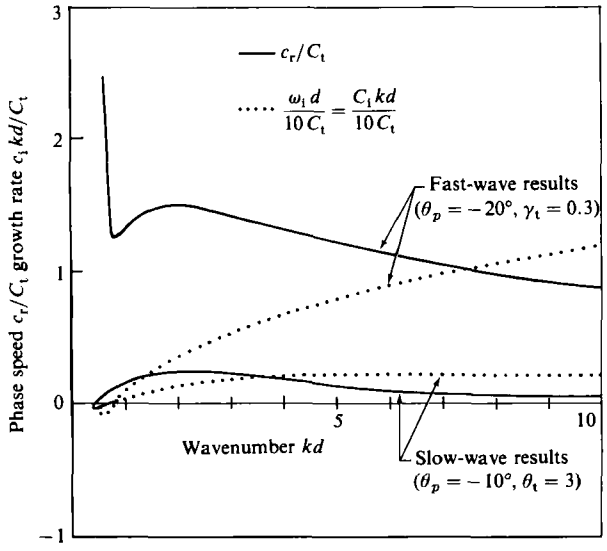

FIGURE 12. Wave speed and growth rate versus wavenumber for comparison with slow and fast wave experimental results – Turbulent boundary layer; $U_\infty/C_t = 8$, $K_p = 0.25$, $\rho_f/\rho_c = 1$.

increasing the viscosity of the fluid in the rotating-disk apparatus.) In the results of Gad-el-Hal *et al.* no waves were found under laminar conditions even at flow speeds as high as $12C_t$. This represents an increase of a factor of 2.7 from their turbulent value. One must consider that this large increase may be due to the disturbance-free character of the towing tank under laminar conditions.

Fast wave results

The experiments of Gad-el-Hak *et al.* mention the appearance of faster waves at high flow speeds. We have attempted to show, at least qualitatively, how these waves might come about. Because of the frequency dependence of the shear-wave speed and relaxation time for plastisol materials, the damping ratio for waves that move with a speed of about C_t would be approximately one order of magnitude less than that for static divergence waves. In figure 12 we compare the dispersion curve for growing slow waves ($\gamma_t = 3$, $K_p = 0.25$, $\theta_p = -10°$) to one for growing fast waves ($\gamma_t = 0.3$, $K_p = 0.25$, $\theta_p = -20°$) at a flow speed of $8C_t$. The slow-wave dispersion curve is qualitatively similar to that in figure 9. The shape of the faster-wave curve is reminiscent of the downstream branch of a Kelvin–Helmholtz or class C instability. Note that the growth rate of the faster waves is everywhere greater than the slow-wave curve, indicating that it would dominate the experimental results.

4. Conclusion

The theory derived in this paper adequately describes some aspects of the dynamics of waves on viscoelastic coatings bounded by a flowing fluid. It has demonstrated the importance of the dimensionless damping parameter γ_t and the phase and magnitude of the surface pressure for the wave behaviour. This simple model, which couples a linear Voigt solid and a modified potential flow, has been used to predict the results of experiments consisting of laminar and turbulent flows over complex viscoelastic coatings. Static divergence, the most frequently observed instability, is

shown to be a damping instability (Benjamin's class A). The model gives reasonable predictions in both magnitude and trend for the onset flow velocity and phase speed of the waves under turbulent conditions and shows that the wavelengths are consistent with a class A wave in this system. The model also predicts a higher onset flow velocity for laminar boundary layers, in qualitative agreement with experiment. It is thought that more accurate predictions could be obtained by increasing the complexity of the flow and solid model without changing the basic physics of the coupling between the two.

This work was supported by the Office of Naval Research under Contract N00014-81-C-0497.

Appendix. Simplifications of the Helmholtz decomposition

In §2 a Helmholtz decomposition was introduced to represent the solid-displacement field as a sum of two parts: an irrotational component (or longitudinal wave) described by the scalar ϕ, and a solenoidal component (or transverse wave) described by the scalar ψ. It was also noted there that ϕ and ψ satisfy (10) and (11):

$$\nabla^2\left(\nabla^2\phi-\frac{1}{C_{\mathrm{L}}^2}\frac{\partial^2\phi}{\partial t^2}\right)\equiv\nabla^2\overline{\Phi}=0,\quad \nabla^2\left(\nabla^2\psi-\frac{1}{C_{\mathrm{T}}^2}\frac{\partial^2\psi}{\partial t^2}\right)\equiv\nabla^2\overline{\Psi}=0. \tag{A 1}$$

Equations (A 1) follow respectively from the divergence and curl of the solid equation of motion. In §2 we assumed $\overline{\Phi}=\overline{\Psi}=0$ and derived the dispersion relation (20). We now prove the validity of this assumption. The decomposition into potential functions must be consistent with the equation of motion itself, which leads to the following two constraints:

$$\frac{\partial\overline{\Phi}}{\partial x}+\frac{C_{\mathrm{T}}^2}{C_{\mathrm{L}}^2}\frac{\partial\overline{\Psi}}{\partial y}=0,\quad \frac{\partial\overline{\Phi}}{\partial y}-\frac{C_{\mathrm{T}}^2}{C_{\mathrm{L}}^2}\frac{\partial\overline{\Psi}}{\partial x}=0. \tag{A 2}$$

Upon solving the Laplace equation (A 1) for $\overline{\Phi}$ and $\overline{\Psi}$, and ensuring satisfaction of the constraints (A 2), we obtain the following forced wave equations for the potential amplitudes $\hat{\phi}(y)$ and $\hat{\psi}(y)$:

$$\left.\begin{aligned}\frac{\mathrm{d}^2\hat{\phi}}{\mathrm{d}y^2}-k^2\alpha^2\hat{\phi}&=\mathrm{i}\Sigma^2(S_1\sinh ky+S_2\cosh ky),\\ \frac{\mathrm{d}^2\hat{\psi}}{\mathrm{d}y^2}-k^2\beta^2\hat{\psi}&=(S_1\cosh ky+S_2\sinh ky),\end{aligned}\right\} \tag{A 3}$$

where

$$\alpha^2\equiv1-\frac{c^2}{C_{\mathrm{L}}^2},\quad \beta^2\equiv1-\frac{c^2}{C_{\mathrm{T}}^2},\quad \Sigma^2\equiv\frac{C_{\mathrm{T}}^2}{C_{\mathrm{L}}^2}.$$

For $c^2\neq0$ we shall demonstrate that $S_1=S_2=0$, in which case (A 3) reduce to (13). With $c^2\neq0$ we have $\alpha^2\neq1$ and $\beta^2\neq1$; hence the solutions of (A 3) take the form

$$\left.\begin{aligned}\hat{\psi}&=\frac{1}{k^2(1-\beta^2)}(S_1\cosh ky+S_2\sinh ky)+S_3\cosh\beta ky+\frac{1}{\beta}S_4\sinh\beta ky,\\ \hat{\phi}&=\frac{\mathrm{i}\Sigma^2}{k^2(1-\alpha^2)}(S_1\sinh ky+S_2\cosh ky)+S_5\cosh\alpha ky+\frac{1}{\alpha}S_6\sinh\alpha ky.\end{aligned}\right\} \tag{A 4}$$

Now the displacement amplitudes, as obtained from (9), are given by

$$\hat{\zeta} = \mathrm{i}k\hat{\phi} + \frac{\mathrm{d}\hat{\psi}}{\mathrm{d}y}, \quad \hat{\eta} = \frac{\mathrm{d}\hat{\phi}}{\mathrm{d}y} - \mathrm{i}k\hat{\psi}. \tag{A 5}$$

Substitution of (A 4) into (A 5) leads to expressions for $\hat{\zeta}(y)$ and $\hat{\eta}(y)$ which contains the six constants S_1, S_6. Requiring that these expressions be compatible with the original equation of motion governing the displacement amplitudes leads to $S_1 = S_2 = 0$ unless $\alpha^2 = \beta^2 = 1$ (i.e. $c^2 = 0$). Thus for $c \neq 0$ the assumption $\overline{\Phi} = \overline{\Psi} = 0$ is proved, and the dispersion relation obtained in §2 is indeed appropriate for unsteady waves.

When $c^2 \equiv 0$, $\alpha^2 = \beta^2 = 1$, and the solutions of (A 3) are

$$\left.\begin{aligned} \hat{\psi}_0 &= \frac{1}{2k}(S_1 y \sinh ky + S_2 y \cosh ky) + S_3 \cosh ky + S_4 \sinh ky, \\ \hat{\phi}_0 &= \frac{\mathrm{i}\Sigma^2}{2k}(S_1 y \cosh ky + S_2 y \sinh ky) + S_5 \cosh ky + S_6 \sinh ky. \end{aligned}\right\} \tag{A 6}$$

Upon substituting (A 6) into (A 5), we obtain expressions for $\hat{\zeta}_0$ and $\hat{\eta}_0$ in terms of the six coefficients $S_1, \ldots, S_6$ again. However, two pairs of coefficients always appear in the form $S_3 + \mathrm{i}S_6$ and $S_4 + \mathrm{i}S_5$, implying that there are really only four independent coefficients. Satisfaction of the four boundary conditions (5)–(8) yields a secular determinant, which upon evaluation yields the following criterion for a static solution $c^2 \equiv 0$:

$$\frac{1}{2}\frac{\rho_{\mathrm{f}}}{\rho}\left(\frac{U_\infty}{C_{\mathrm{t}}}\right)^2 \mathrm{e}^{\mathrm{i}\theta_p} = \frac{1 + \Sigma^4 + (1-\Sigma^4)\cosh 2kd + 2(1-\Sigma^2)^2 (kd)^2}{(1+\Sigma^2)\sinh 2kd - (1-\Sigma^2)\,2kd}. \tag{A 7}$$

In the limit of an incompressible solid, $\Sigma^2 \to 0$.

It is straightforward but tedious to show that condition (A 7) is contained in the dispersion relation (20). By expanding (20) in powers of c, for small c, one obtains (A 7) as the coefficient of the c^4 term. Thus (20) is also correct for $c = 0$. Expression (A 7) determines where along the kd-axis the C_{f} and C_{i} curves simultaneously cross zero. For $\theta_p = 0$ this condition occurs at real values of kd. For $\theta_p \neq 0$ the C_{r} and C_{i} curves do not cross zero at the same real value of kd.

REFERENCES

Balasubramanian, R. & Orszag, S. A. 1983 Numerical studies of laminar and turbulent drag reduction. *NASA Contract Rep.* 3669.

Benjamin, T. B. 1959 Shearing flow over a wavy boundary. *J. Fluid Mech.* **6**, 161–205.

Benjamin, T. B. 1960 Effects of a flexible boundary on hydrodynamic stability. *J. Fluid Mech.* **9**, 513–532.

Benjamin, T. B. 1963 The threefold classification of unstable disturbances in flexible surfaces bounding inviscid flows. *J. Fluid Mech.* **16**, 436–450.

Benjamin, T. B. 1964 Fluid flow with flexible boundaries. In *Proc. 11th Intl Congr. Appl. Mech., Germany*, pp. 109–128.

Bushnell, D. M., Hefner, J. N. & Ash, R. L. 1977 The effect of compliant wall motion on turbulent boundary layers. *Phys. Fluids* **20**, 531–548.

Chyu, W. J. & Au-Yang, M. K. 1973 Response of panels to turbulence-induced surface-pressure fluctuations and resulting acoustic radiation to the flow field. *AIAA Paper* 73-993, *AIAA Acoustics Specialists Conf., Seattle.*

Delves, L. M. & Lyness, J. N. 1967 A numerical method for locating the zeros of an analytic function. *Maths Comp.* **21**, 543–560.

DOWELL, E. H. 1975 *Aeroelasticity of Plates and Shells.* Noordhoff.

DUNGUNDJI, J., DOWELL, E. & PERKIN, B. 1963 Subsonic flutter of panels on continuous elastic foundations. *AIAA J.* **1**, 1146.

FUNG, Y. C. 1965 *Foundations of Solid Mechanics.* Prentice-Hall.

GAD-EL-HAK, M., BLACKWELDER, R. F. & RILEY, J. J. 1984 On the interaction of compliant coatings with boundary-layer flows. *J. Fluid Mech.* **140**, 257–280.

GISLASON, T. 1971 Experimental investigation of panel divergence at subsonic speeds. *AIAA J.* **9**, 2252–2258.

HANSEN, R. J. & HUNSTON, D. L. 1974 An experimental study of turbulent flows over compliant surfaces. *J. Sound Vib.* **34**, 297–308.

HANSEN, R. J. & HUNSTON, D. L. 1983 Fluid-property effects on flow-generated waves on a compliant surface. *J. Fluid Mech.* **133**, 161–177.

HANSEN, R. J., HUNSTON, D. L., NI, C. C., REISCHMAN, M. M. & HOYT, J. W. 1979 Hydrodynamic drag and surface deformations generated by liquid flows over flexible surfaces. In *Viscous Flow Drag Reduction; Prog. Astro. Aero.* **72**, 439–451.

HUNSTON, D. L., YU, C. & BULLMAN, G. W. 1984 Mechanical properties of compliant coating materials. In *Laminar and Turbulent Boundary Layers*, vol. 11 (ed. E. M. Uran & H. E. Weber). New York: ASME.

KENDALL, J. M. 1970 The turbulent boundary layer over a wall with progressive waves. *J. Fluid Mech.* **14**, 259–281.

LANDAHL, M. T. 1962 On the stability of a laminar incompressible boundary layer over a flexible surface. *J. Fluid Mech.* **13**, 609–632.

LANDAHL, M. T. & KAPLAN, R. E. 1965 Effect of compliant walls on boundary layer stability and transition. *AGARDograph* 97-1-353.

MILES, J. W. 1956 On the aerodynamic instability of thin panels. *J. Aero. Sci.* **23**, 771–791.

RAYLEIGH, LORD 1885 On waves propagated along the plane surface of an elastic solid. *Proc. Lond. Math. Soc.* **17**, 4–11.